NIST Technical Note 2107

Development of a Kinematic Measurement Method for Knee Exoskeleton Fit to a User

Roger Bostelman
Ya-Shian Li-Baboud
Karl Van Wyk
Mili Shah

This publication is available free of charge from:
https://doi.org/10.6028/NIST.TN.2107

National Institute of Standards and Technology
U.S. Department of Commerce

NIST Technical Note 2107

Development of a Kinematic Measurement Method for Knee Exoskeleton Fit to a User

Roger Bostelman
Smart HLPR, LLC

Ya-Shian Li-Baboud
National Institute of Standards and Technology
Information Technology Laboratory

Karl Van Wyk
NVIDIA
Artificial Intelligence Robotics Research Laboratory

Mili Shah
The Cooper Union for the Advancement of Science and Art
Mathematics Department

This publication is available free of charge from:
https://doi.org/10.6028/NIST.TN.2107

August 2020

U.S. Department of Commerce
Wilbur L. Ross, Jr., Secretary

National Institute of Standards and Technology
Walter Copan, NIST Director and Undersecretary of Commerce for Standards and Technology

National Institute of Standards and Technology Technical Note 2107
Natl. Inst. Stand. Technol. Tech. Note 2107, 23 pages (August 2020)
CODEN: NTNOEF

This publication is available free of charge from:
https://doi.org/10.6028/NIST.TN.2107

Abstract

Proper exoskeleton fit to user impacts the safety of the human robot interaction. Exoskeletons are now being marketed by several manufacturers and yet there are currently no defined methods to measure the exoskeleton fit to the user. This research aims to develop a quantifiable test and measurement framework for evaluating exoskeleton performance, beginning with the tracking of knee kinematics. Key challenges in knee kinematic measurements include the complexity of human biomechanics, the variability of human anthropometry as well as the uncertainty of marker position, relative to underlying skeletal features, as computed by an optical tracking system (OTS). A measurement methodology to assess exoskeleton-to-leg fit based on comparison of knee kinematics between the human and the exoskeleton is proposed. The methodology is based on the use of rigid artifacts to minimize marker motion, and therefore measurement error. Separate artifacts for the exoskeleton and the human limbs enable independent tracking of exoskeleton and knee joint kinematics in order to assess exoskeleton fit to user. A prosthetic test apparatus and a 3D printed human knee model apparatus were also designed and developed to simulate the biomechanics of the human knee. The experimental data from the prosthetic leg test apparatus showed agreement with both the simulated analytical model and the ground truth skeletal structure relative to the artifacts placed on the simulated leg. The reconfigurable artifact was also tested by the researchers to demonstrate how the novel design can be used to track knee kinematics between the human leg and the exoskeleton leg.

Key words

exoskeleton; knee kinematics; optical tracking system; measurement error; reconfigurable artifact; testbed.

Table of Contents

List of Tables

List of Figures

1. Introduction

As exoskeletons are being adopted for industrial use, their long-term effects remain unknown. Exoskeletons are now being marketed by several manufacturers and yet there are currently limited methods to measure exoskeleton fit to user [1]. To address this industry gap, the National Institute of Standards and Technology (NIST) has begun developing test methods for exoskeletons [2]. We begin with kinematic alignment of exoskeleton to human limb, which impacts the load and overall safety of human robot interaction [3]. We began with lower extremity (leg) fit in our assessment of the exoskeleton fit. Wearable or adherable test platforms for reconfigurable marker placement, also referred to as test "artifacts," were designed and built at NIST for use with an optical tracking system (OTS). NIST also designed and built a test apparatus with tibial, knee, and femoral components, allowing researchers to compare the alignment of the exoskeleton and human test artifacts to a skeletal leg frame. A simulated ground truth (GT) test apparatus joined by a prosthetic knee and subsequently a 3D printed knee as well as a test methodology for knee joint exoskeletons are presented in this paper. The artifact development was also intended to advance metrology on the safety and performance of exoskeletons. Key metrics for evaluating the fit to user of exoskeletons include the ability of the exoskeleton to move in concert with the human and the ability to minimize resistance between the human-machine interface to maintain comfort and reduce fatigue [4]. In this initial work, we focus primarily on comparing the exoskeleton and the user knee kinematics, with the underlying assumption that the greater the similarity of the two kinematic trajectories, the better the exoskeleton fits the user.

Methodologies for tracking knee kinematics have been developed using various types of sensors, including electrogoniometric apparatus, optical motion analysis systems, rate gyroscopes and accelerometers [5][6]. Inertial measurement units (IMUs) have knee joint angle estimation errors of up to 4° [7]. Regardless of the sensors used, three significant challenges for developing such methodologies are (1) the development of a quantifiable set of metrics to evaluate exoskeleton performance [8]; (2) the complexity and variability of human joint motions; and (3) the uncertainty of sensing and measurement systems.

An OTS, while subject to limitations, currently provides the most accurate data sets for measuring the position and rotation of rigid bodies [9]. Previous studies using OTS typically require skin-mounted markers, where marker position uncertainty relative to the skeletal frame can be up to 55 mm [10]. Skin-mounted markers also require greater computational complexity to compensate for error contributions from motions in the muscle and adipose tissues [11][12]. Additionally, human joints rely on a combination of the muscles, tendons, and bones for movement, rendering joint location a challenge to estimate accurately. Moreover, knee kinematics do not have a fixed axis of rotation and are subject to the variations in the surfaces of the joint between the femoral condyle and the tibial condyle [13][14]. In addition to using OTS, research on markerless methods is ongoing in analyzing and predicting three-dimensional (3D) joint motion from two-dimensional (2D) images [15][16][17][18][19]. Many of the markerless methods are based on annotated images for determining joint position estimation error. Developing a method to optimize marker stability using the OTS could potentially provide a more consistent basis to evaluate markerless methods.

This paper describes a proposed test methodology and metrics to address the following gaps in exoskeleton research: (1) quantification of exoskeleton performance evaluation and (2) characterization of the human and the exoskeleton interactions. The contributions of this initial evaluation include: (1) developing a set of test artifacts to independently track the exoskeleton and knee kinematics with an OTS using rigid test artifacts that accommodate variations in human anthropometry, (2) providing accurate, computationally-efficient algorithms to characterize exoskeleton and human knee kinematics, and (3) improving understanding of the sources and magnitude of error of the proposed exoskeleton test methodology on two test apparatus used to simulate human knee biomechanics. The test artifacts are defined as the engineered attachments for reconfigurable marker placement to the human and exoskeleton limbs. The human and exoskeleton artifacts developed for this study enable the placement of retroreflective markers to form a rigid body for OTS tracking. The rigid body artifacts developed for this study are intended to reduce extraneous motions from pliable surfaces. Instead of directly applying markers to the subject, the subject wore the human artifacts, which provided the markers a rigid structure and asymmetrical marker placement, therefore reducing the OTS tracking errors. Similarly, the exoskeleton artifacts were attached to the exoskeleton limb to track the exoskeleton kinematics. The independent computations of the human knee joint and exoskeleton knee joint trajectory can be used to derive metrics for the exoskeleton knee joint fit to user and to determine the ergonomic support provided by the exoskeleton.

2. Experiments

Three experiments were performed to determine if the measurement and analysis methods outlined in this paper provided sufficient information about the exoskeleton fit to the user. The experiments involved the use of: 1) a prosthetic knee test apparatus, 2) a 3D printed knee test apparatus, and 3) a human subject. The three experiments are detailed in the following subsections.

2.1. Prosthetic Knee Apparatus

Initially, a simulated leg apparatus was designed and built using aluminum bars and an off-the-shelf prosthetic knee. Two exoskeleton artifacts, made of aluminum plates on which four markers were mounted in asymmetrical patterns, were then strapped, using bungee cords, to both sides of the tibia (see Fig. 1). The prosthetic knee, developed based on knee and ankle joint biomechanics, provided a sample basis for understanding the knee kinematics. The skeletal frame had markers attached directly to the apparatus to provide a centerline. The markers attached to the skeletal frame provided simple computation of the tibia and femur center lines. The skeletal center lines served as the basis for determining the ground truth (GT) angle of the knee extension and flexion. For the prosthetic knee apparatus, the exoskeleton artifacts were applied to determine the feasibility of using the test artifacts to measure the full range of knee motion and for developing analytical approaches to model knee kinematics. The bungee cord provides a flexible means to attach test artifacts to either the exoskeleton or the human limbs. The test apparatus can therefore be used to evaluate the stability of the bungee cord as a means of attaching the artifact to the subject or the exoskeleton.

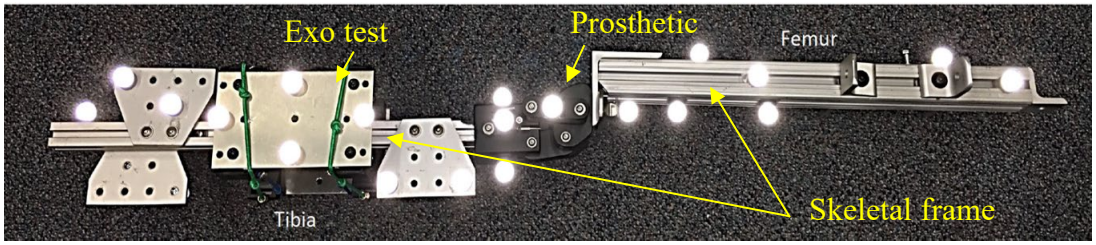

(a)

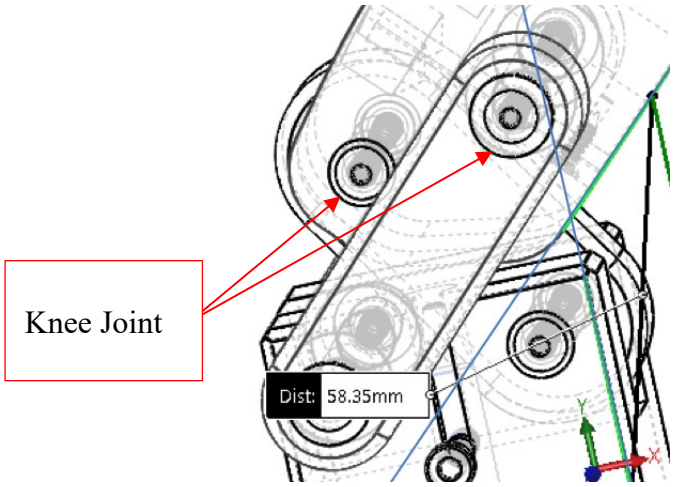

(b)

Fig. 1. (a) Initial test apparatus with two exoskeleton artifact plates on both sides of the tibia, and two skeletal frames to simulate the femur and the tibia attached with a prosthetic knee. (b) Prosthetic knee joint with a pair of rolling pins to provide the linear and rotational components human knee joint biomechanics.[1]

Four retroreflective markers were adhered to each of the exoskeleton artifacts in a non-colinear pattern in order to optimize the accuracy of the OTS computation of each marker's 3D position. The prosthetic knee's measured range of motion was approximately 0º to 130º relative to the femur. With the prosthetic knee test apparatus, the OTS captured 46 static measurements ranging from 0º to 130º in increments ranging 7º to 15º taken for a duration of 10 s at a capture rate of 120 frames per second (fps).

2.2. 3D Printed Knee Apparatus

A second apparatus was designed and built to include a 3D printed knee. The NIST 3D human knee computer aided design (CAD) model was extrapolated to be approximately 30% larger than a 2D CAD model of a real knee [20]. The larger model was intended to amplify the linear motion of the knee biomechanics. Attached to the 3D printed knee were two aluminum bars to simulate the femur and tibia, providing the skeletal frame. Fig. 2(a) shows a CAD model of the 3D printed knee biomechanically similar to a human knee, with

[1] *Certain commercial entities, equipment, or materials may be identified in this document in order to describe the experimental procedure adequately. Such identification is not intended to imply recommendation or endorsement by the National Institute of Standards and Technology, nor is it intended to imply that the entities, materials, or equipment are necessarily the best available for the purpose.*

rotational and translational components. The 3D CAD model isolates motion to the sagittal plane, the longitudinal plane dividing the left and right sides of the body. The 3D printed knee model includes both rotational and linear motion similar to human knee motion having non-circular bone-to-bone (with cartilage) motion. The model uses a center axis screw that moves along a linear slot (see Fig. 2(a)) along with an outer screw that rotates in a circular slot having two tangential curves of different radii such that their rotation axes model the biomechanics of the human knee.

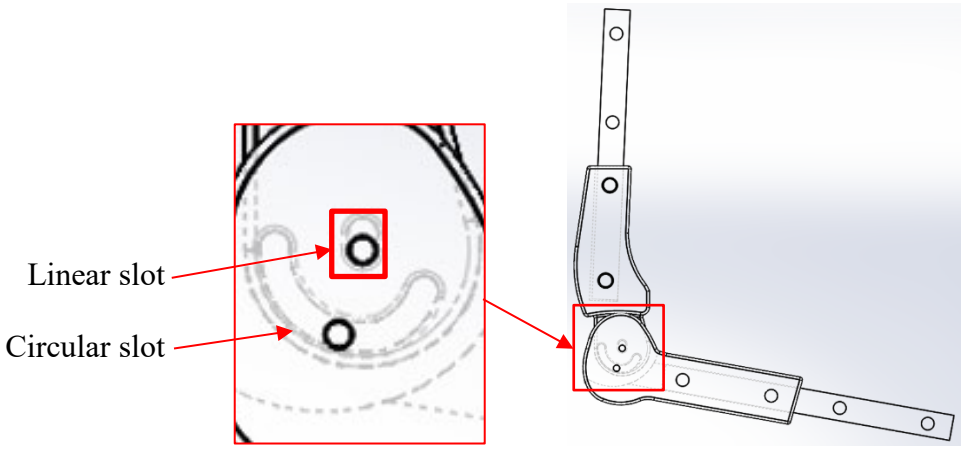

Fig. 2. The design model of the 3D printed knee test apparatus, where (a) highlights the printed knee design's rotational and translational components of the knee kinematics and (b) shows the skeletal frame to which the artifacts can be attached.

Two exoskeleton (Exo) artifacts were attached to one side of the tibia and femur using bungee cords. In addition, two human test artifacts, designed and 3D printed at NIST were rigidly attached using screws to the tibia and femur bars as shown in Fig. 3. The test artifacts enabled reconfigurable attachment of markers and are intended to be worn on the test subject for tracking the knee joint kinematics. Each artifact plate included four markers mounted and adjusted to asymmetrical patterns to ensure unique OTS capture of individual markers. The human artifacts are fixed to the skeletal frame using brackets and double-sided adhesive so they can be easily moved as needed. The human artifacts were intended to allow a comparison with no relative motion to the femur and tibia bars on which ground truth markers were attached. The placements of the Exo artifacts were intended to compare the kinematics derived from the Exo artifacts relative to the ground truth skeletal frame and the human artifacts. Ground truth markers were attached using double-sided tape to the bars on all four sides of the bar providing a simple bar centroid computation. The comparison of the kinematics is used to establish the test system error, bias and uncertainty, based on the physically-simulated human knee motion.

The artifacts were rectangular and designed to align relative to the tibia and femur bars. As shown in Fig. 3, the artifact placement was designed to align with the tibia and femur positions in order to capture the translational and rotational motions of the knee joint.

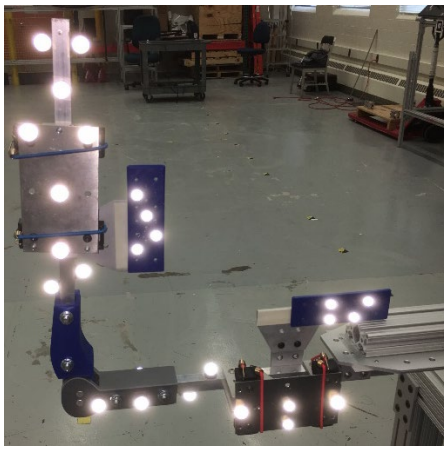

Fig. 3. Human femur and tibia artifacts mounted at an offset from the femur and tibia bars. Exo femur and tibia artifacts, with markers, approximately aligned with the skeletal frame. Individual markers were also fixtured to the tibia and femur bars and used for determining the skeletal center line (ground truth).

Similar to the experiment with the prosthetic knee, the experiment with the 3D printed knee test apparatus was intended to capture the full flexion and extension of the knee biomechanics. Static data was acquired using the OTS measuring the artifacts relative locations in the test space to determine the artifact error for knee rotation angle. Fifty trials were performed using the 3D printed knee apparatus. The measured knee joint angle ranged from full extension, 0°, to full flexion, measured at approximately 130°. The data for each trial was taken using an OTS at static increments ranging from 3° to 15° for 10 s at a capture rate of 120 fps. An angle meter was used to obtain an approximate correlation of the leg angles, to the OTS measurements of the apparatus bars, human artifacts, and exoskeleton artifacts.

It would be difficult for a human to move and hold their leg at various angles to acquire static data of artifacts strapped onto their leg and fixtured to the exoskeleton. Therefore, after static measurements were completed, dynamic measurements of the skeletal frames attached with prosthetic and 3D printed knees were performed by manually moving the tibia from full extension to full flexion several times to see if the full range of continuous motion can be accurately captured by tracking the joint angles or distances between the artifacts. The dynamic apparatus motion would be similar the extension and flexion kinematics of knee bends for a human.

2.3. Reconfigurable Human Mounts

After confirming that the human and Exo artifacts could reasonably capture the motion of the simulated tibia and femur of the devices, the next experiment was to design a human leg attachment apparatus to support the human artifact to an exoskeleton user's leg. Reconfigurable mounts for actual human-attachment were designed and 3D printed as shown in Fig. 4. Fig. 4 shows the mounts and elastic (bungee) straps used to mount it to the user. The mounts are designed to comfortably attach and conform to a variety of human leg shapes and sizes. To complete the preliminary validation, a user also wore the exoskeleton while wearing the human artifacts and Exo artifacts were mounted to the exoskeleton as shown in Fig. 4(b).

The OTS was re-calibrated for the limb artifact tests. At least three trials of dynamic motions, three sets of knee bends per trial, were obtained for each of the prosthetic, the printed knee and the human experiments.

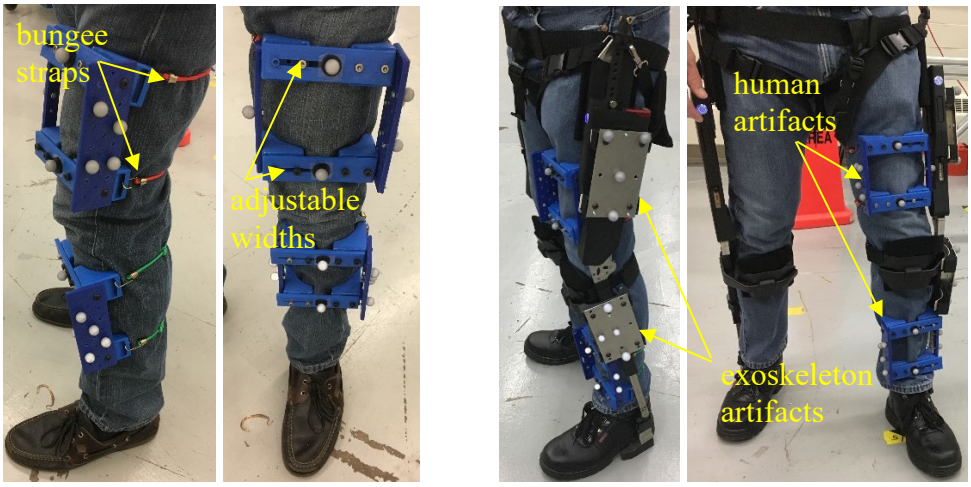

(a) (b)

Fig. 4. (a) Sagittal and frontal views of the reconfigurable human artifacts attached to a human leg. (b) Human artifacts attached to human leg and Exo artifacts attached to an exoskeleton. The two front markers could also be used as mount alignment to the leg and to compare the alignment between artifacts.

3. Results

3.1. Analytical Model of Knee Kinematics

The analysis of the exoskeleton artifacts' static positions confirms the artifacts are able to capture the rotational and linear components of the knee kinematics due to the rolling and sliding interactions between the knee joints. The motion of the prosthetic knee and the 3D printed knee were mathematically modeled based on CAD specifications and physical measurements.

OTS marker data along with a digital caliper and a measuring tape were used to approximate the knee angles and the distance between the reference point on the tibia from the knee center position (Fig. 5) to establish the kinematic trajectory from the static data as shown in Fig. 6(a). Fig. 6(a) shows the alignment of the static measurements for the prosthetic knee test apparatus with respect to the simulation fit. P0, P1, and P2 positions are derived from the OTS marker data. In addition, the knee center position (P0, as denoted in Fig. 5) uses the caliper measurements of the inner and outer rolling attachment points. The lengths, $\ell_L = \|P2 - P0\|$ along the *x-axis,* and $\ell_H = \|P2 - P1\|$ along the $y - axis,$ are measured with a measuring tape. The simulation fit was modeled based on the trajectory of the rolling pins. We observed that the static data points were aligned with the rotational trajectory of the simulation, but the model did not capture the linear shift in the trajectory.

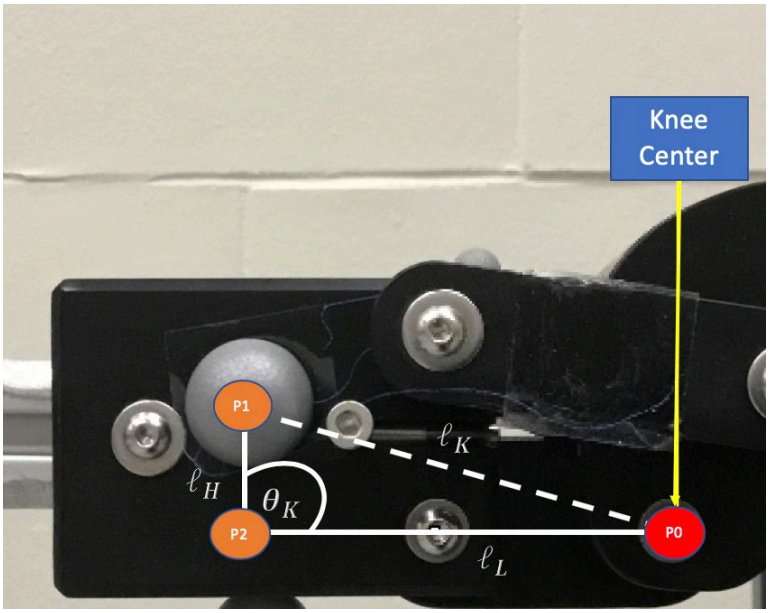

Fig. 5. Illustration of how the approximations for ℓ_K are derived for each static measurement of the prosthetic knee.

The static data points are based on distances derived from the variable length of the knee, ℓ_K, which is approximated using the cosine law as shown (1), in addition to the tibia length, which is derived from the tibia center position, , C_τ, in 2D. C_τ is approximated based on the mean 3D position computations from the OTS, using both artifact plates on each side of the tibia.

$$\ell_K = \sqrt{\ell_H^2 + \ell_L^2 + 2\ell_L\ell_H \cos\theta_K} \qquad (1)$$

With the 3D printed knee developed at NIST, the exact angle at which the linear shift occurs can be determined based on the CAD model. The linear shift, defined as the translation of the radius due to the linear motion of the knee joint, as highlighted in Fig. 6(b), was a subtle increase of about 3.25 mm in the tibial radius during flexion indicating the shift of the pin in the linear slot of the 3D printed knee. The non-shift, defined as the rotational motion of the knee joint, shows the trajectory of the simulated motion prior to and after the shift of the pin in the linear slot. The rotational trajectory of the static data points during flexion is rendered by the circular slot.

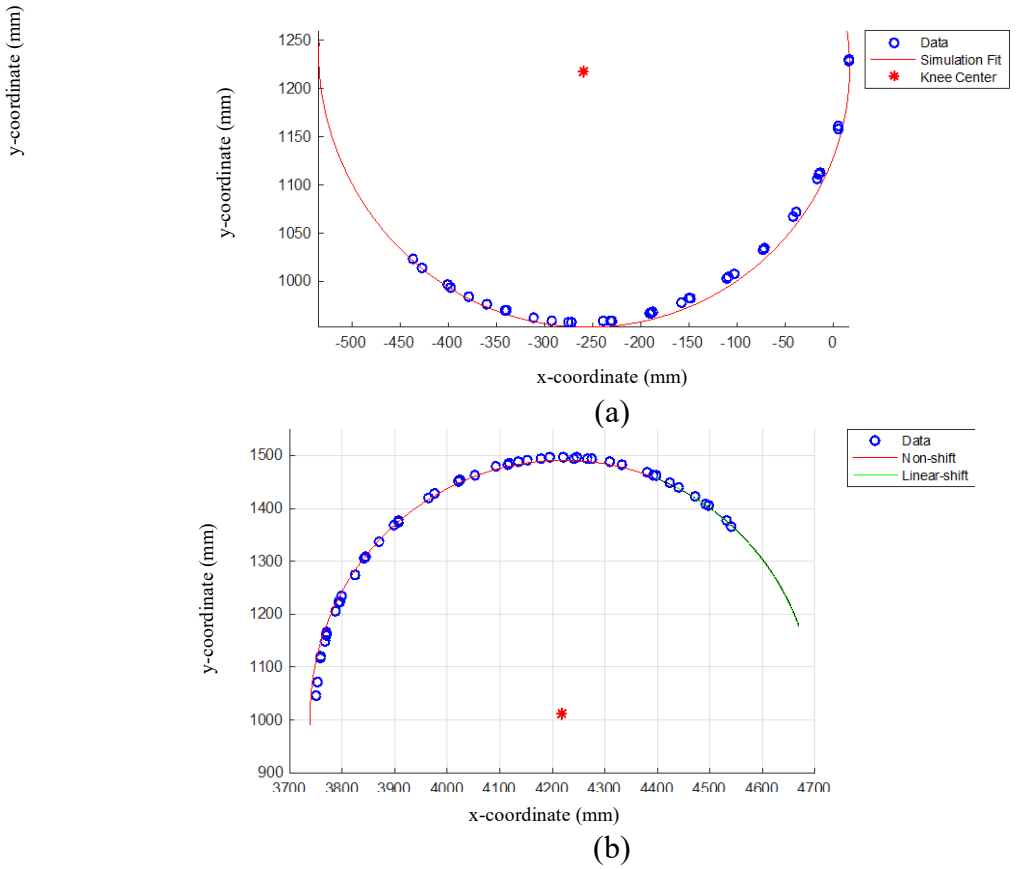

Fig. 6. (a) Prosthetic and (b) 3D printed knee simulation fit with tibia position data based on 46 and 50 static trials, respectively.

3.2. Evaluation of the Artifact-Based Test and Measurement Methodology

The baseline OTS GT joint angle measurement was compared with measurements from an angle meter, measured by the same operator to maximize repeatability. The commercial off-the-shelf angle meter had a specified accuracy of ± 0.2° and a repeatability of ± 0.05°. The measurement bias and uncertainty between the OTS and the angle meter measurements were found to be 1.3° ± 0.9° on the prosthetic configuration. The bias can be attributed to the different locations where the angle was determined. The aggregated uncertainty can be attributed to OTS error, angle meter error, and operator error.

$$knee_{flexion}° = tan^{-1} \frac{\|\overrightarrow{femur} \times \overrightarrow{tibia}\|}{\overrightarrow{femur} \cdot \overrightarrow{tibia}} \quad (2)$$

From the initial findings, the experiment was modified to include artifacts on both the tibia and femur for the 3D printed knee experiments. The artifact placement provided a higher fidelity capture of the knee motion as a combination of the two skeletal components.

The objective of the 3D printed knee analysis was to determine the accuracy and stability of the Exo artifacts to the skeletal bars (GT) and the human artifacts to the GT. For each set of GT, Exo artifact, and human artifact markers, the rigid body markers were used to establish a vector at the femur and a vector at the tibia as shown in Fig. 7. The angle between the two vectors was computed using (2), where the GT angle was used to compare the angle measurements based on the angle meter and the OTS.

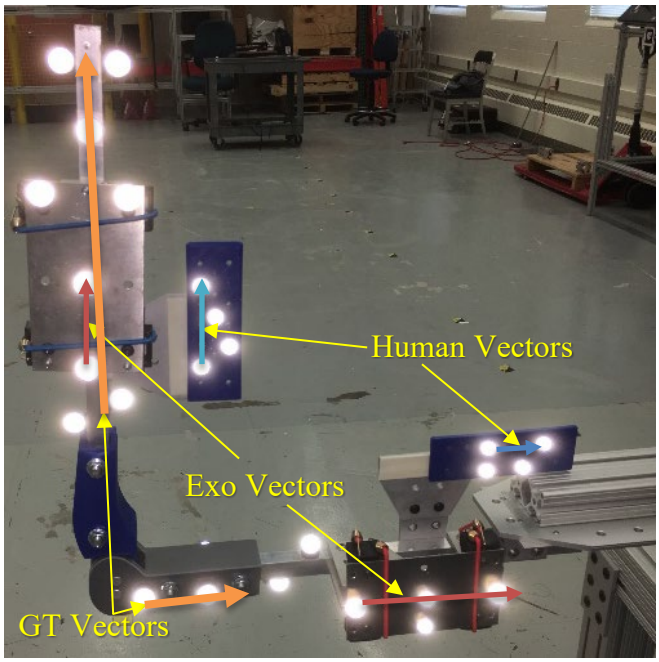

Fig. 7. Femur and tibia vectors, based on rigid body markers, used for the GT (green), Exo (orange), human (blue) knee flexion angle computations.

The static results from the leg test apparatus based on the 3D printed knee enabled the algorithm development. The first method was to compare the alignment of the Exo and human artifacts to the ground truth from the markers on the bars as well as the measured angle. Several metrics were devised to determine the reliability and the error in angle estimation based on the artifact versus the ground truth. Table 1 compares the mean standard deviation (σ_μ), maximum standard deviation (σ_{max}), and minimum standard deviation (σ_{min}) *amongst* the 50 trials for the Exo artifacts, human artifacts and the GT bars. Factors contributing to the uncertainties include OTS measurement uncertainty, test apparatus stability, and artifact stability.

Table 1. Analysis of artifact angle variation between the 50 trials on the printed knee apparatus.

	σ_μ (°)	σ_{max} (°)	σ_{min} (°)
GT	0.013	0.058	0.005
Exo	0.082	0.359	0.009
Human	0.106	0.261	0.026

Table 2 compares the correlation coefficients between the artifacts and the GT and the measured values. The Exo artifact was highly correlated (r = 0.999) with both the measured and GT values as it was aligned with the bar. The angle differences between the GT and Exo artifacts ranged from 0.31º to 1.41º, while the angle differences between the GT and human artifacts ranged from 0.14º to 2.17º for the 50 trials. The static analysis demonstrated the exoskeleton artifacts are aligned within 1º to 2º to the GT based on the 50 trials, as shown in Fig. 8.

Table 2. Angle difference between artifact and ground truth with the printed knee.

	$R_{AngleMeter}$	R_{GT}	$\|GT\text{-}Artifact\|_{\mu}$ (º) [σ]	$\|GT\text{-}Artifact\|_{max}$ (º)	$\|GT\text{-}Artifact\|_{min}$ (º)
GT	0.9994	1.0000	-	-	-
Exo	0.9995	0.9999	0.805 [0.35]	1.413	0.312
Human	0.8980	0.8973	1.179 [0.55]	2.167	0.136
Angle Meter	1.0000	0.9994	1.365 [1.66]	3.667	0.013

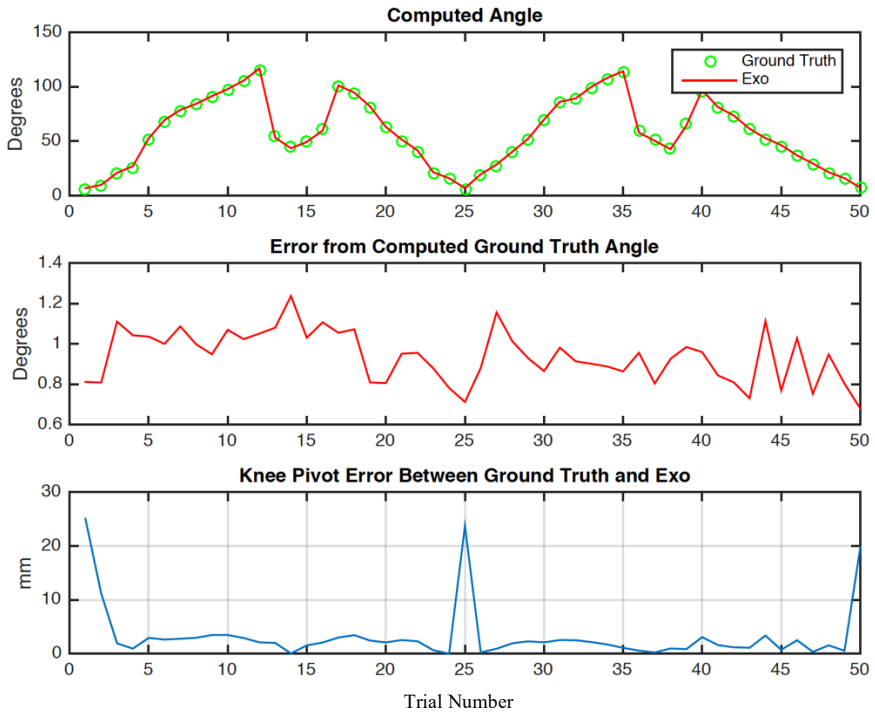

Fig. 8. Comparison of exoskeleton artifacts and computed ground truth.

Fig. 9 shows how the angles from the human and Exo artifacts track the GT angles in a dynamic trial. There was a larger angle bias when the apparatus is held at the extremities, indicating a need to verify the knee center approximation in order to minimize the angle bias

based on the vectors derived from the artifact markers. The standard deviation of the angle offset is used to estimate the error, which ranges from 1.1º to 1.3º.

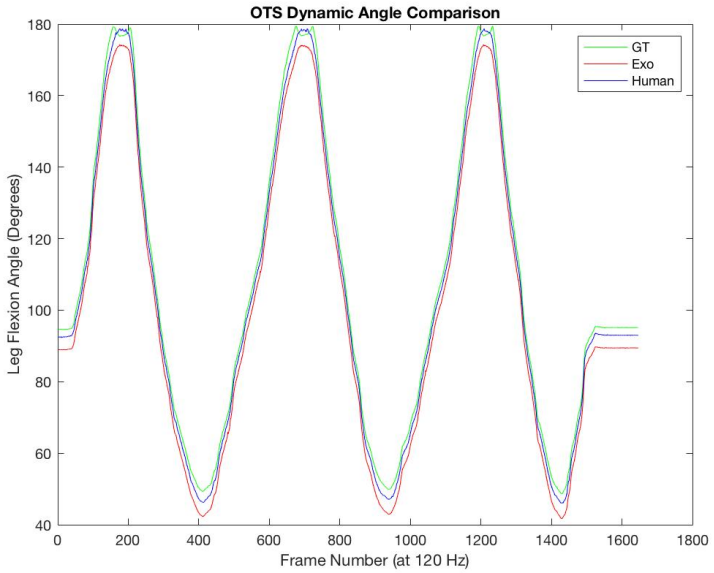

Fig. 9. Comparison of exoskeleton and human artifacts with skeletal frame (GT) angles for a dynamic trial.

Table 3 compares the rotation angle differences between the bars based on the OTS (GT) and the angle meter measurement with the rotation angle between human and Exo artifacts.

Table 3. Angle estimation difference between artifact and angle meter.

	Exo Artifact Angle Error (°)		**Human Artifact Angle Error (°)**	
	Angle Meter	OTS	Angle Meter	OTS
Static	[1.61]	[0.35]	[1.66]	[0.55]
Dynamic	-	[1.25]	-	[1.10]

A distance-based performance metric, $\|m_t - m_f\|$, was developed to track the Euclidean distance between the centroids of the femoral and tibial artifacts with the distance between the GT centroids:

$$\|m_t - m_f\| = \sqrt{(x_t - x_f)^2 + (y_t - y_f)^2 + (z_t - z_f)^2} \qquad (3)$$

The analysis used $\|m_t - m_f\|$ to track the knee kinematics as shown in Fig.10.

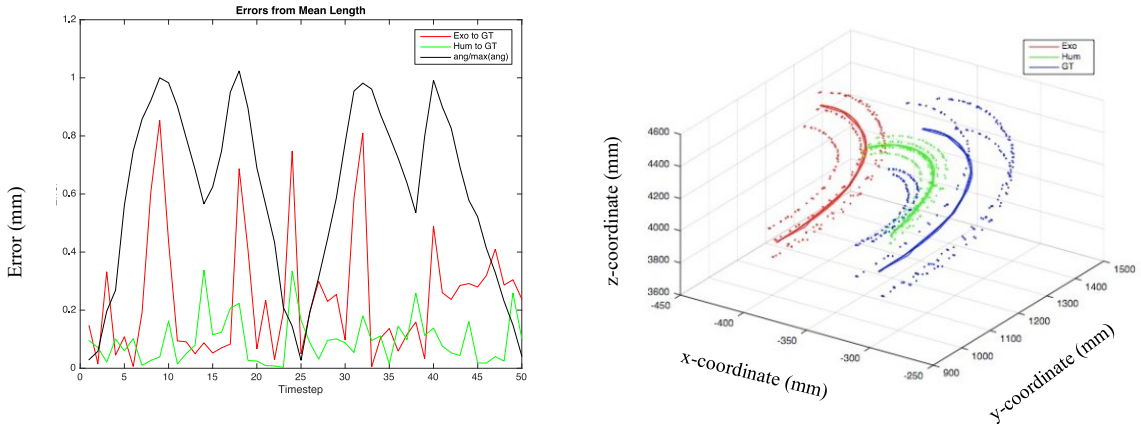

(a) (b)

Fig. 10. Artifact distance (a) offsets from GT based on the femur and tibia centroids over the dynamic set and (b) trajectory over the static and dynamic data sets.

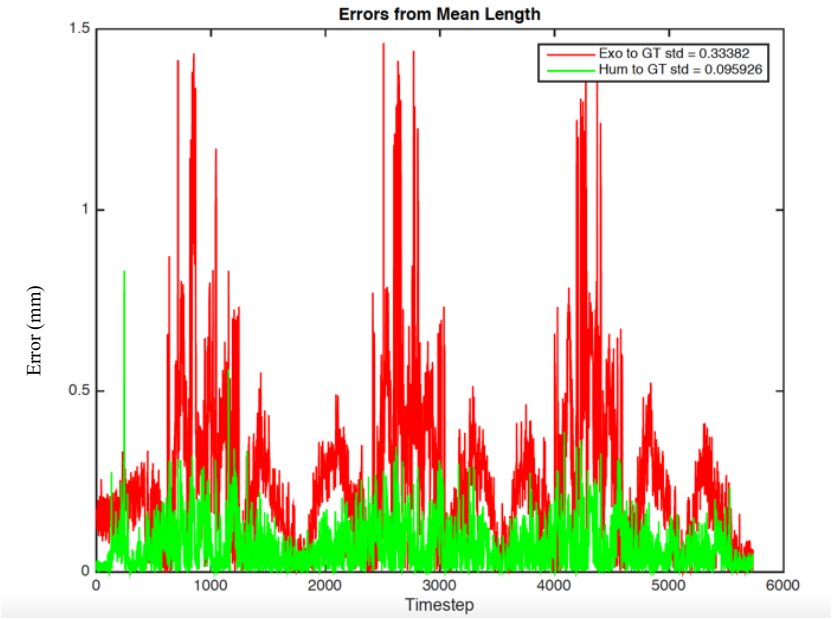

Fig. 11. Dynamic errors (in mm) based on artifact distance using the 3D printed knee test apparatus from a single trial.

The knee kinematics of the dynamic trial experiment is shown in Fig. 11, Fig. 12 for the prosthetic knee apparatus, and Fig. 13 for the printed knee apparatus. For the printed knee with both human and Exo artifacts, the standard deviation was:

- 0.33 mm: standard deviation of the distance between the centroid of the tibia markers for the Exo and the centroid of the GT tibia markers.
- 0.13 mm: standard deviation of the distance between the centroid of the tibia markers for the human and the centroid of the GT tibia markers.

These differences in the standard deviation showed the stability of the artifact attachment. The Exo artifacts were attached to the skeletal frame by bungee cords, while the human artifacts were more rigidly attached to the skeletal frame with screws.

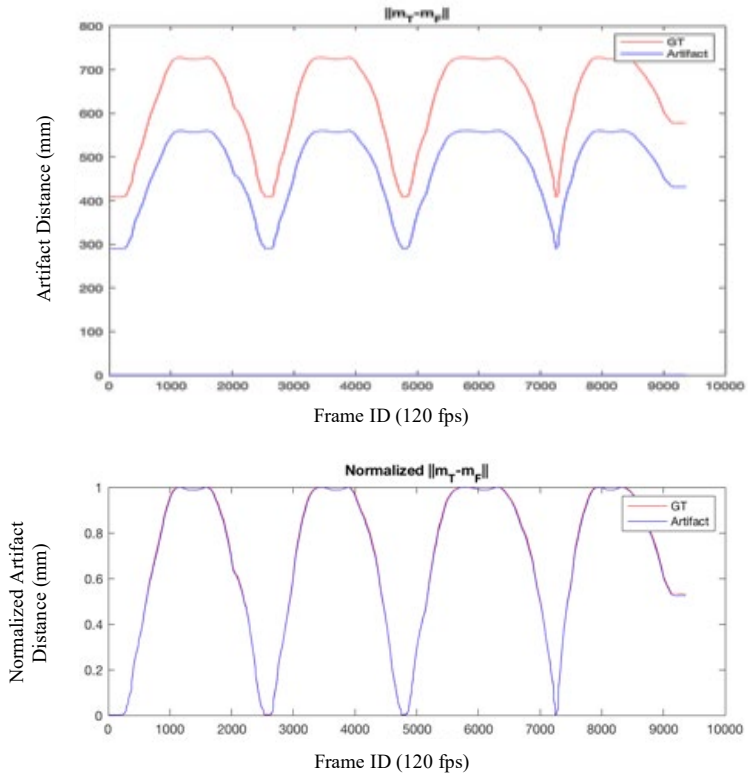

Fig. 12. Motion tracking of knee kinematics, showing agreement between the GT tibial-femoral lengths and the artifact lengths for the prosthetic knee test apparatus.

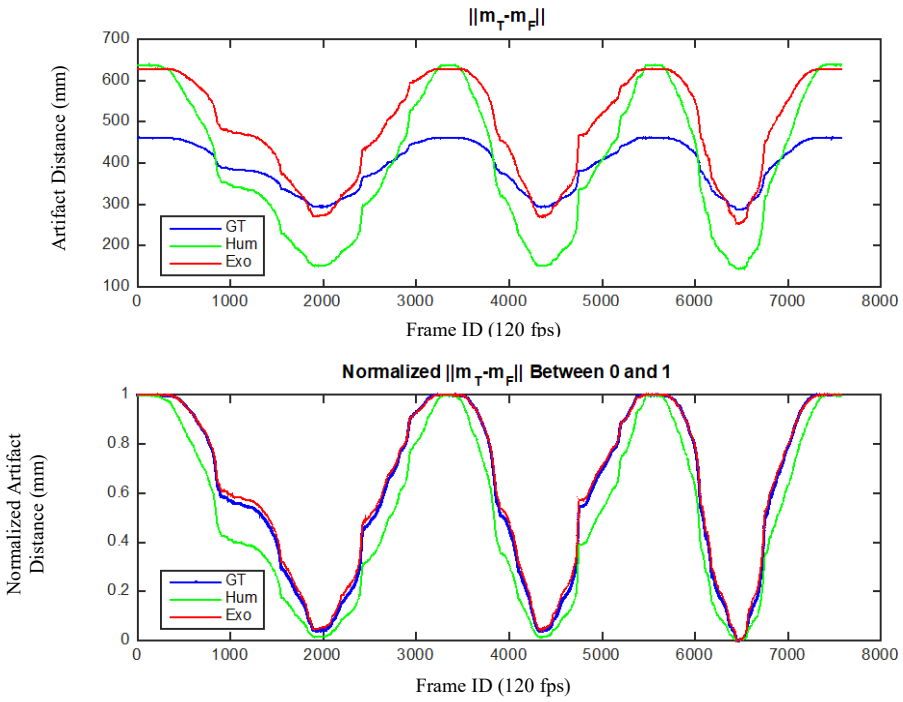

Fig. 13. GT and artifact distances (in mm) can be used to track the knee kinematics in the 3D printed knee test apparatus.

One of the key metrics is the ability of the exoskeleton to move in concert with the human kinematics in order to minimize the force on the human. Hence, the experiment with the prosthetic knee and 3D printed knee test apparatus provided the basis of the human knee biomechanics. The Exo artifacts would track the exoskeleton kinematics independent of the human knee joint kinematics. Therefore, when an exoskeleton is worn by the human wearing both the human and Exo artifacts, both the exoskeleton and human knee kinematics can be tracked to assess exoskeleton fit to user.

A full exoskeleton experiment was then performed with both Exo artifacts mounted to a passive (non-powered) exoskeleton and human artifacts mounted to the user as the user performed squats.

Fig. 14 shows the relative movement of the human to exoskeleton motions as measured (Fig. 14a) and normalized (Fig. 14b). When normalized, the exoskeleton and human kinematics correlated relatively well during the knee flexion and extension phases (i.e., going from a standing position to a squat and back to a standing position) of the subject, which demonstrated the potential usefulness of the independent human and Exo artifact measurement method. Several phenomena occurred during the extension phase, as shown in the graphs in Fig. 14, highlighted with the blue boxes, including:

- the subject raised the heels during knee flexion contributing to the second peak during knee flexion from standing to squatting,

- the bungee cords used to strap the human artifacts to the subject had some rotational and translational movements during extension,
- the human and Exo artifacts move forward and back during the top of the squatting motion where fluctuation in femur/tibia distance measurements occur. The flat portion of the graph, as emphasized in Fig. 14a, shows the consistent distance when the exoskeleton springs were engaged/disengaged providing a visual indication of the exoskeleton's resistance force on the subject.

Since Fig. 14 shows that, when normalized to each other, the human artifact centroids overlay graph data on the exoskeleton artifact centroids and throughout the squat phase (i.e., the time when the exoskeleton aids the user), the measurement and analysis methods are able to track the exoskeleton's alignment to the user's leg.

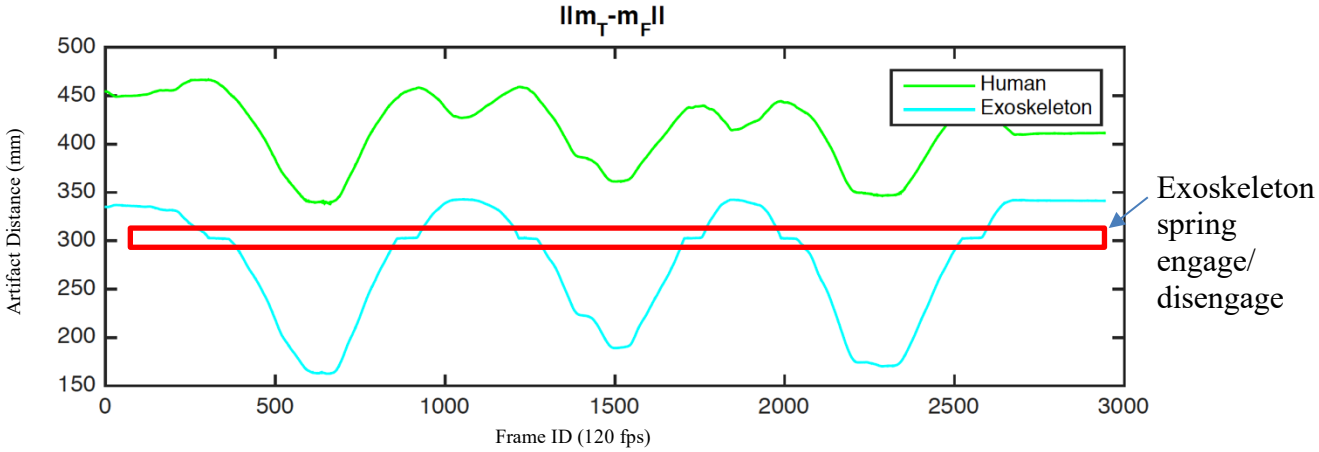

(a)

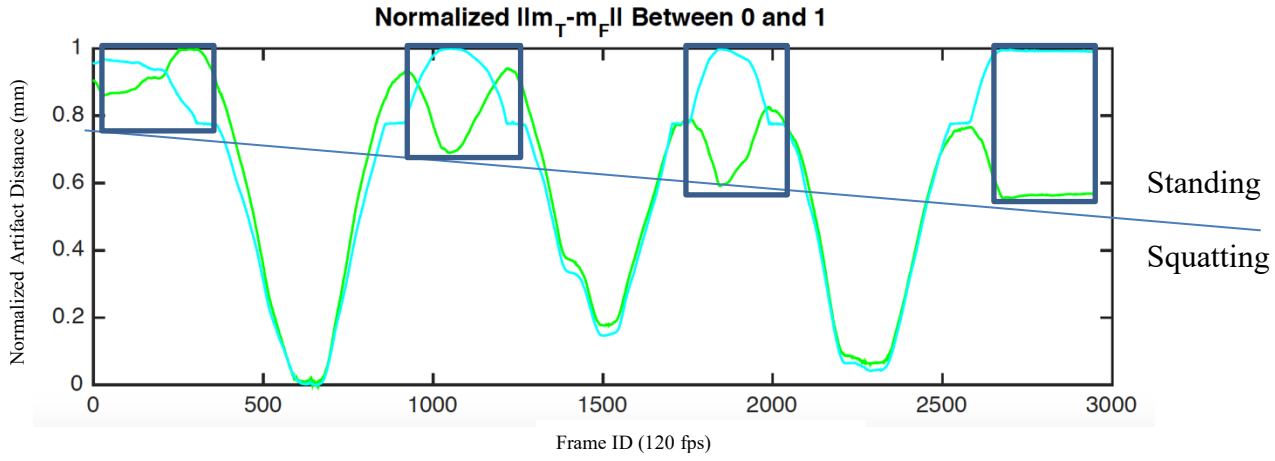

(b)

Fig. 14. Limb test based on the distance between the tibia and femur centroids for human and Exo artifacts (a) and with the normalized distances. (b) The blue boxes are phenomena that occur during leg extension, when the user goes from a squat to a standing position.

4. Conclusions

Exoskeletons are being used by industry even as long-term effects of their use are unknown and there are no defined methods to measure the exoskeleton fit to the user. The study focused on improving marker-based measurement methods for establishing the feasibility of using exoskeleton and human artifacts to track knee kinematics first by using rigid skeletal frames joined by a prosthetic and a 3D printed knee. When the artifacts are positioned in line with the skeletal frame, the kinematic trajectories of the artifacts follow the GT trajectory. Towards a measurement method on human subjects, NIST experimented with the use of artifacts strapped onto a human and attached to an exoskeleton both of which were measured using an OTS. As the two artifact types were independently attached, the relative motion between the exoskeleton and human limb can be measured and analyzed. The artifacts provided relatively minimal skin and muscle movement impact on measurements. Some muscle movement did cause human artifact rotation upon knee extension. Attachment of the human artifact using bungee cords needs to be replaced to minimize the artifact's rotational motion.

The prosthetic knee and 3D printed knee test apparatus verified a potential measurement method to assess exoskeleton fit to user based on knee kinematics. This opens up the possibilities of using them for a wide range of applications. The experimental results indicated minimal relative movement between the Exo and human artifacts with respect to ground truth. Our study was limited to the assessment of a marker-based methodology using artifacts attached to the skeletal test apparatus. Future studies are needed to compare the fidelity of the human artifact-based measurement method to the direct placement of markers on the human subjects. In the subsequent human subjects' study, where subjects have varying anthropometry and biomechanics, the motion capture data and analysis could provide further determination on the impact of the artifacts on joint angle measurement uncertainty. Motion capture data from the study could also provide a ground truth basis for comparison of tracking accuracy in markerless exoskeleton evaluation methods. Markerless methods are more conducive in providing a flexible test framework for manufacturing facilities by allowing testing to be done in actual manufacturing environments with less hindrance for the user, and less cost to the manufacturing company.

5. References

[1] De Looze, M.P., Bosch T., Krause F., Stadler K.S., and O'Sullivan L.W. (2016) "Exoskeletons for industrial application and their potential effects on physical work-load." *Ergonomics,* 59(5), pp. 671-681.

[2] Bostelman R. and Hong T. (2018) "Test Methods for Exoskeletons–Lessons Learned from Industrial and Response Robotics." *Wearable Exoskeleton Systems: Design, Control and Applications. The Institution of Engineering Technology*, 13, pp. 335-361.

[3] Schiele, A. (2009) "Ergonomics of exoskeletons: Objective performance metrics." *IEEE World Haptics 2009-Third Joint EuroHaptics conference and Symposium on Haptic Interfaces for Virtual Environment and Teleoperator Systems*, pp. 103-108.

[4] Steger R., Kim S.H., and Kazerooni H. (2006) "Control scheme and networked control architecture for the Berkeley lower extremity exoskeleton (BLEEX)."

(2006) *Proceedings 2006 IEEE International Conference on Robotics and Automation*, pp. 3469-3476.
[5] Laubenthal, K.N., Smidt, G.L., and Kettelkamp, D.B. (1972) "A quantitative analysis of knee motion during activities of daily living." *Physical therapy,* 52(1), pp. 34-43.
[6] Van den Bogert, A.J., Read, L., and Nigg, B.M. (1996) "A method for inverse dynamic analysis using accelerometry." *Journal of Biomechanics,* 29(7), pp. 949-954.
[7] Bergmann, J.H., Mayagoitia, R.E., and Smith, I.C. (2009) "A portable system for collecting anatomical joint angles during stair ascent: a comparison with an optical tracking device." *Dynamic Medicine,* 8(1), pp.3.
[8] Cenciarini, M. and Dollar, A.M. (2011) "Biomechanical considerations in the design of lower limb exoskeletons." *2011 IEEE International Conference on Rehabilitation Robotics*, pp. 1-6.
[9] Mayagoitia, R.E., Nene, A.V., and Veltink, P.H. (2002) "Accelerometer and rate gyroscope measurement of kinematics: an inexpensive alternative to optical motion analysis systems." *Journal of biomechanics* 35(4), pp. 537-542.
[10] Aurand, A.M., Dufour, J.S., and Marras, W.S. (2017) "Accuracy map of an optical motion capture system with 42 or 21 cameras in a large measurement volume." *Journal of biomechanics,* 58, pp. 237-240.
[11] Leardini, A., Chiari, L., Della Croce, U., and Cappozzo, A. (2005) "Human movement analysis using stereophotogrammetry: Part 3. Soft tissue artifact assessment and compensation." *Gait & posture,* 21(2), pp. 212-225.
[12] Garling, E.H., Kaptein, B.L., Mertens, B., Barendregt, W., Veeger, H.E.J., Nelissen, R.G., and Valstar, E.R. (2007) Soft-tissue artefact assessment during step-up using fluoroscopy and skin-mounted markers. *Journal of Biomechanics* 40:S18-S24.
[13] Cappozzo, A., Catani, F., Leardini, A., Benedetti, M.G., and Della Croce, U. (1996) "Position and orientation in space of bones during movement: experimental artefacts", *Clinical biomechanics*, 11(2), pp. 90-100.
[14] Akhter, I. and Black, M.J. (2015) Pose-conditioned joint angle limits for 3D human pose reconstruction. Proceedings of the IEEE Conference on Computer Vision and Pattern Recognition, pp1446-1455.
[15] Joo, H., Simon, T., and Sheikh, Y. (2018) "Total capture: A 3d deformation model for tracking faces, hands, and bodies." *Proceedings of the IEEE Conference on Computer Vision and Pattern Recognition*, pp. 8320-8329.
[16] Mathis, A., Mamidanna, P., Cury, K.M., Abe, T., Murthy, V.N., Mathis, M.W., and Bethge, M. (2018) "DeepLabCut: markerless pose estimation of user-defined body parts with deep learning." *Nature Neuroscience,* 21(9), pp. 1281-1289.
[17] Omran, M., Lassner, C., Pons-Moll, G., Gehler, P., and Schiele B. (2018) "Neural body fitting: Unifying deep learning and model based human pose and shape estimation." *2018 International Conference on 3D Vision (3DV)*, pp. 484-494.
[18] Pellis, G. (2018) *Knee Top Joint research*. Retrieved from http://it.ktj.it/index.html. *Accessed August 3, 2020.*
[19] Pavlakos, G., Choutas, V., Ghorbani, N., Bolkart, T., Osman, A., Tzionas, D., and Black, M.J. (2019) "Expressive body capture: 3d hands, face, and body from a

single image." *Proceedings of the IEEE Conference on Computer Vision and Pattern Recognition*, pp. 10975-10985.
[20] Wang, D., Lee, K.M., Guo, J., and Yang, C.J. (2014) "Adaptive knee joint exoskeleton based on biological geometries." *IEEE/ASME Transactions on Mechatronics*, 19(4), pp.1268-1278.